15. Zeilinger, A., Horne, M. A., Weinfurter, H. & Zukowski, M. Three-particle entanglements from two entangled pairs. *Phys. Rev. Lett.* **78,** 3031–3034 (1997).
16. Rarity, J. G. & Tapster, P. R. Three-particle entanglement from entangled photon pairs and a weak coherent state. *Phys. Rev. A* **59,** R35–R38 (1999).
17. Pan, J.-W., Simon, C., Brukner, C. & Zeilinger, A. Entanglement purification for quantum communication. *Nature* **410,** 1067–1070 (2001).
18. Knill, E., Laflamme, R. & Milburn, G. J. A scheme for efficient quantum computation with linear optics. *Nature* **409,** 46–52 (2001).
19. Bouwmeester, D. Bit-flip-error rejection in optical quantum communication. *Phys. Rev. A* **63,** R040301 (2001).
20. Hein, M., Eisert, J., & Briegel, H.J. Multi-party entanglement in graph states. *Phys. Rev. A* **69,** 06231 (2004).
21. Briegel, H. J & Raussendorf, R. Persistent entanglement in arrays of interacting particles. *Phys. Rev. Lett.* **86,** 910–913 (2001).
22. Kwiat, P. G. *et al.* New high intensity source of polarization-entangled photon pairs. *Phys. Rev. Lett.* **75,** 4337–4341 (1995).
23. Kurtsiefer, C. *et al.* A step towards global key distribution. *Nature* **419,** 450 (2002).
24. De Martini, F., Buzek, V., Sciarrino, F. & Sias, C. Experimental realization of the quantum universal NOT gate. *Nature* **419,** 815–818 (2002).
25. Pan, J.-W., Gasparoni, S., Rupert, U., Weihs, G. & Zeilinger, A. Experimental entanglement purification of arbitrary unknown states. *Nature* **423,** 417–422 (2003).
26. Zukowski, M., Zeilinger, A. & Weinfurter, H. Entangling photons radiated by independent pulsed source. *Ann. NY Acad. Sci.* **755,** 91–102 (1995).
27. Pittman, T. B., Jacobs, B. C. & Franson, J. D. Probabilistic quantum encoder for single-photon qubits. *Phys. Rev. A* **69,** 042306 (2004).
28. Zukowski, M. & Kaszlikowski, D. Critical visibility for N-particle Greenberger-Horne-Zeilinger correlations to violate local realism. *Phys. Rev. A* **56,** R1682–R1685 (1997).
29. Bouwmeester, D. *et al.* Experimental quantum teleportation. *Nature* **390,** 575–579 (1997).
30. Pittman, T. B., Jacobs, B. C. & Franson, J. D. Demonstration of nondeterministic quantum logic operations using linear optical elements. *Phys. Rev. Lett.* **88,** 257902 (2002).

**Acknowledgements** This work was supported by the National Natural Science Foundation of China, the Chinese Academy of Sciences, the National Fundamental Research Program and the German Research Foundation (DFG).

**Competing interests statement** The authors declare that they have no competing financial interests.

**Correspondence** and requests for materials should be addressed to J.-W.P. (jian-wei.pan@physi.uni-heidelberg.de).

# Cyclotron frequency shifts arising from polarization forces

**James K. Thompson, Simon Rainville & David E. Pritchard**

*Research Laboratory of Electronics, MIT-Harvard Center for Ultracold Atoms, and Department of Physics, Massachusetts Institute of Technology, 77 Massachusetts Avenue, Cambridge, Massachusetts 02139, USA*

**The cyclotron frequency of a charged particle in a uniform magnetic field $B$ is related to its mass $m$ and charge $q$ by the relationship $\omega_c = qB/m$. This simple relationship forms the basis for sensitive mass comparisons using ion cyclotron resonance mass spectroscopy, with applications ranging from the identification of biomolecules[1] and the study of chemical reaction rates[2] to determinations of the fine structure constant of atomic spectra[3]. Here we report the observation of a deviation from the cyclotron frequency relationship for polarizable particles: in high-accuracy measurements of a single $CO^+$ ion, a dipole induced in the orbiting ion shifts the measured cyclotron frequency. We use this cyclotron frequency shift to measure non-destructively the quantum state of the $CO^+$ ion. The effect also provides a means to determine to a few per cent the body-frame dipole moment of $CO^+$, thus establishing a method for measuring dipole moments of molecular ions for which few comparably accurate measurements exist[4–6]. The general perturbation that we describe here affects the most precise mass comparisons attainable today[7,8], with applications including direct tests of Einstein's mass–energy relationship[9] and charge-parity-time reversal symmetry[10], and possibly the weighing of chemical bonds[7].**

The cyclotron frequency shift reported here for an ion with electric polarizability $\alpha$ can be understood using the exaggerated microscopic picture shown in Fig. 1. As the molecule (with net charge indicated by $+$ ) moves on its cyclotron orbit (solid circle) with velocity $\mathbf{v}$ perpendicular to the magnetic field $\mathbf{B}$, the Lorentz force is experienced in its instantaneous rest frame as a motional electric field $\mathbf{E}_m = \mathbf{v} \times \mathbf{B}$. The motional electric field induces a dipole $\mathbf{d}_{ind} = \alpha \mathbf{E}_m$ (modelled here by the outer $+$ and $-$ charges), which points towards the centre of the cyclotron orbit. As the ion orbits, the orientation of the induced dipole adiabatically follows the motional electric field (as indicated by the two snapshots at times $t$ and $t + \Delta t$). As a result, the two ends of the induced dipole move at slightly different speeds (as emphasized by the dashed lines). The differential velocity gives rise to a net additional Lorentz force on the particle that is also directed along the radial direction. The size of the induced dipole is proportional to the ion's velocity, which for the circular cyclotron motion is proportional to its cyclotron radius. A constant frequency shift then results because the size of the additional Lorentz force scales linearly with the cyclotron radius, just as the original Lorentz force does. Equivalently, the cyclotron frequency shift occurs because the induced dipole moves the centre of charge to a radius different from that of the centre of mass. The fractional frequency shift is then simply given by the ratio of the distance between the two centres and the cyclotron radius.

This polarization force also occurs for neutral particles, and can be generally modelled as a renormalization of the inertial mass of the particle in the plane perpendicular to the magnetic field. If a neutral particle accelerates, the induced dipole relaxes to a new equilibrium value, creating a transient Lorentz force that either opposes or enhances the change in velocity, acting like a changed inertial mass. The new effective mass is given simply by $m_\lambda = m(1 + \alpha_\lambda B^2/m)$ where $m$ is the usual inertial mass, and $\alpha_\lambda$ is the electric polarizability of the particle. This expression for the effective mass can be derived by including a phenomenological polarization

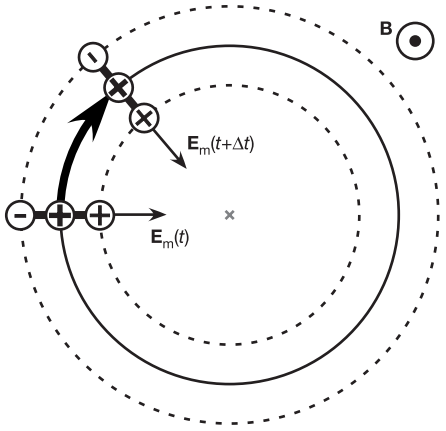


**Figure 1** An exaggerated microscopic picture of the polarization force shift of the cyclotron frequency. As the molecule (with net charge indicated by $+$ ) moves on its cyclotron orbit (solid circle) perpendicular to the magnetic field $\mathbf{B}$, the magnetic field is experienced in its instantaneous rest frame as a motional electric field $\mathbf{E}_m$. The motional electric field induces a dipole (modelled here by the outer $+$ and $-$ charges), which points towards the centre of the cyclotron orbit. As the ion orbits, the orientation of the induced dipole adiabatically follows the motional electric field (as indicated by the two snapshots at times $t$ and $t + \Delta t$). As a result, the two ends of the induced dipole move at slightly different speeds (as emphasized by the dashed lines) thus generating an additional Lorentz force. The orbital frequency then has to adjust in order to compensate for the additional force.

energy in the lagrangian, as was first pointed out in the context of neutral atom interferometry[11]. Since the polarizability may depend on the quantum state of the particle, it carries a label $\lambda$ to specify the state. A key result here is that the effective mass $m_\lambda$, as determined from the measured cyclotron frequency $\omega_c^\lambda = qB/m_\lambda$, depends on the quantum state of the particle through the polarizability. For the present work, the fractional modification of the cyclotron frequency with respect to that for a particle of the same mass and charge but zero polarizability is $\Delta\omega_c{}^\lambda/\omega_c = -\alpha_\lambda B^2/m \approx 10^{-9}$. Note that this is a fundamental shift of the cyclotron frequency, in contrast to shifts arising from experimental artefacts (such as the image charge shift or the quadrupole electric field used to confine the ions along the magnetic field lines during the measurement). This cyclotron frequency shift has not been previously recognized or observed, but it is crucial to consider for a precision better than $10^{-9}$, which is now being approached by several groups[7,8,10,12].

Experimentally, magnetic field noise limits the ability to observe the expected changes in the cyclotron frequency $\Delta\omega_c{}^\lambda/\omega_c$. Instead, we measure the ratio of cyclotron frequencies for two different ions (only one of which is polar). For the best discrimination against magnetic and other sources of noise on the ratio, we recently developed a technique to confine the two different ions in a Penning trap and simultaneously compare their cyclotron frequencies, as is described in ref. 7. With this novel technique, we can obtain mass ratios with fractional accuracies below $10^{-11}$.

Quantum-state-dependent polarization shifts of the cyclotron frequency are clearly observable in the time evolution of the cyclotron frequency ratio of a single $CO^+$ and a single $N_2^+$ (see Fig. 2a). The ratio changes by $\sim 10^{-9}$ in discrete jumps between approximately three values, remaining stable for many hours

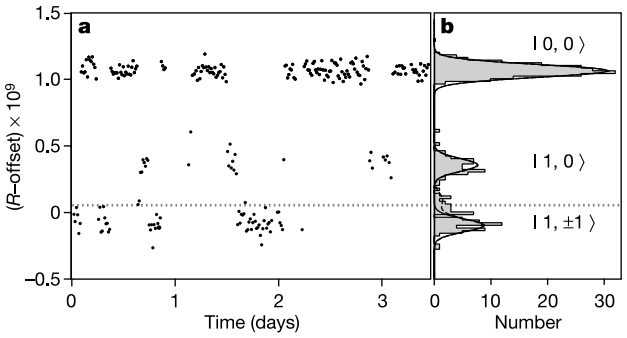


**Figure 2** The cyclotron frequency ratio $R = \omega_c[N_2^+]/\omega_c[CO^+]$. **a**, Measured versus time, and **b**, a histogram of all measured values. The subtracted offset is our previously measured ratio $R = 0.999\,598\,887\,572$ (determined by alternately trapping the two ions[20]). The ratio changes when the $CO^+$ ion absorbs or emits a black-body photon and jumps to a quantum rotational state with a different electric polarizability. The many hour lifetimes of the states and the fraction of time spent in each state are in reasonable agreement with the calculated values (see Table 1). The spectrum of measured ratios has three main components, as is made more clear by the histogram in **b**, which includes additional data not shown in **a**. The separation between the dominant three peaks allows the rotational state $|N,M_N\rangle$ of the $CO^+$ molecule to be non-destructively determined from a single ratio measurement. The curves are fits to determine the molecular dipole moment $\mu$ and the cyclotron frequency ratio unperturbed by polarization forces. The solid line includes only contributions from $N = 0$ and 1 (reduced chi-square $\chi_\nu^2 = 1.1$), while the dashed line also includes small contributions from the $N = 2$ rotational states ($\chi_\nu^2 = 0.8$). The fits have the following adjustable parameters: the unperturbed cyclotron frequency ratio $R$, the dipole moment $\mu$, a common gaussian width arising from the measurement noise, and a separate amplitude for each gaussian. The grey dashed line indicates the final unperturbed ratio $R$ as reported in the text. The quoted errors on the parameters $\mu$ and $R$ were conservatively increased to reflect small variations resulting from, for example, changing the binning and including only two of the three states at a time in the fit.

between the jumps. That the variation was of the $CO^+$ cyclotron frequency, and not of the $N_2^+$, was confirmed by directly observing the individual cyclotron frequencies of both the $CO^+$ and $N_2^+$ using a magnetometer to remove external magnetic field fluctuations—a technique sufficient for coarsely identifying jumps of order $10^{-9}$. Additionally, the measured cyclotron frequency ratio of the symmetric molecules $N_2^+$ and $^{13}C_2H_2^+$ (which have much smaller polarizabilities than the asymmetric $CO^+$) did not manifest any jumps[7,13].

We considered and eliminated many possible experimental artefacts as being the source of the jumps. We developed techniques to measure precisely the orbits of the simultaneously confined ions and found no correlation between the jumps and changes in their orbits (which coupled with our magnetic field inhomogeneity might give rise to jumps of the observed magnitude). Also, the size and rate of the jumps does not vary with ion–ion separation, counter-indicating Coulomb interactions as a source of the jumps. Combined with numerous other checks, we feel confident that the observed jumps in the cyclotron frequency ratio are not experimental artefacts of our technique for accomplishing simultaneous cyclotron frequency comparisons.

The ratio jumps because the cyclotron frequency of the $CO^+$ molecule changes when it absorbs or emits black-body radiation and moves from one quantum rotational state to another. To interpret the observed data, one must first know that the $CO^+$ and $N_2^+$ molecules are trapped for many days, giving the $CO^+$ time to come to thermal equilibrium with the 4.2 K environment of the trap. At this temperature, the $CO^+$ is in the ground electronic and vibrational state and spends the majority of its time in the lowest few rotational levels. The states with total angular momentum $N = 0$ and 1 will be shown to give rise to the three distinct cyclotron frequencies observed.

To determine the best basis in which to calculate the expected cyclotron frequency shifts, we first consider the hierarchy of energy scales. The $CO^+$ ion possesses an unpaired electron whose spin strongly couples to the 8.5 T magnetic field resulting in a set of independent spin up and spin down manifolds. A much smaller spin-rotation coupling $\hbar\gamma_e\mathbf{S}\cdot\mathbf{N}$, with coupling constant $\gamma_e/2\pi = 0.57$ GHz, fixes the quantization axis for the rotational states along the spin quantization axis, that is, the magnetic field direction ($\hbar$ is the reduced Planck's constant)[14]. The energy splitting between rotational levels $N$ and $N+1$ is given by $E_{N,N+1} = 4\pi\hbar B_0(N+1)$, with the rotational constant $B_0 = 58.983$ GHz (ref. 14).

In the ion's instantaneous rest frame, the motional electric field arising from the cyclotron motion appears to rotate in the $x$–$y$ plane at the cyclotron frequency $\omega_c/2\pi \approx 4.67$ MHz. The interaction is quasi-static because $E_{N,N+1}/\hbar$ and $\gamma_e$ are both much larger than $\omega_c$; hence, the induced dipole adiabatically rotates with the motional electric field. In addition, a typical cyclotron radius of $\rho_c = 75\,\mu$m gives a motional electric field $E_m = 190\,\mathrm{V\,cm^{-1}}$, and polarization

Table 1 **Calculated and measured properties for $CO^+$**

| State | | $\alpha_\lambda$ | $\Delta\omega_c^\lambda/\omega_c$ ($10^{-12}$) | | $\tau$ (h) | | Occupation | |
|---|---|---|---|---|---|---|---|---|
| $N$ | $M_N$ | ($10^{-38}\,\mathrm{C\,m^2\,V^{-1}}$) Th. | Th. | Exp. | Th. | Exp. | Th. | Exp. |
| 0 | 0 | 63.14 | −988 | −1008(30) | 6.3 | 7(3) | 0.54(6) | 0.65 |
| 1 | 0 | 18.96 | −297 | −302(9) | 2.4 | - | 0.14(9) | 0.16 |
| 1 | ±1 | −9.462 | 148 | 151(5) | 2.4 | 4(2) | 0.28(11) | 0.19 |
| 2 | | <4.5 | <70 | - | 0.04 | - | 0.04 | - |

The theoretical (Th.) values are calculated using $\mu = 1.015ea_0$. The experimental (Exp.) fractional cyclotron frequency shifts $\Delta\omega_c^\lambda/\omega_c$ are from the fit shown in Fig. 2b. The calculated lifetimes $\tau$ include both spontaneous and thermally induced transition rates at 4.2 K. The occupation is the fraction of the total time spent in each state as calculated from the normalized Boltzmann weights at 4.2 K. The uncertainties on the theoretical occupation values (given in parentheses) account for the finite observation time of approximately 4 days compared to the theoretical transition rates. Values indicated by – are not quoted owing to insufficient data.

energies of only $V_p = -\frac{1}{2}\alpha_\lambda E_m^2 \leq 2\pi \times 0.17\,\mathrm{MHz}$. Hence, we are justified in using the d.c. polarizability calculated using standard second-order time-independent perturbation theory, in which the molecular dipole moment squared enters as an overall scale factor[15].

For the pertinent two lowest rotational levels, the above model predicts three distinct values of the polarizability. These can be understood qualitatively as follows (see Table 1 for the quantitative results.) The motional electric field, lying in the $x$–$y$ plane, only couples states $|N, M_N\rangle$ and $|N', M'_N\rangle$ for which $N' - N = \pm 1$ and $M'_N - M_N = \pm 1$. Thus, the state $|0,0\rangle$ and pair of states $|1 \pm 1\rangle$ repel one another leading to opposite signs of the polarizability between the ground state and these two excited states. Meanwhile, the state $|1,0\rangle$ does not interact with the ground state, but is repelled downwards by the pair of states $|2, \pm 1\rangle$ so that its polarizability has the same sign as $|0,0\rangle$, but a smaller magnitude owing to the larger energy denominator and smaller Clebsch-Gordon coefficients.

The calculated free space lifetimes of the states (including thermally induced transition rates) are in good agreement with the observed lifetimes (Table 1). In Fig. 2a, the observed transitions between $|1,0\rangle$ and $|1,\pm 1\rangle$ (which would violate parity) are explained by pairs of transitions to and back from a state $|2, M_N\rangle$. These transitions are not clearly resolved owing to the short lifetime of 3 min for $N = 2$ states, whereas the ratio is averaged over the typical 5 min comparison interval.

The above model quantitatively accounts for the observed distribution of cyclotron frequency ratios, and can be used to determine accurately the molecular dipole moment of $CO^+$ and the unperturbed mass ratio $R = M[CO^+]/M\left[N_2^+\right]$. A histogram is made of the number of times each cyclotron frequency ratio is measured (Fig. 2b.) A simultaneous fit to the dominant three peaks, in which the molecular dipole moment acts as a scale factor while the ratio of the intervals between the peaks is held fixed by theory, yields a good reduced chi-squared of $\chi^2_\nu = 1.1$ (see solid curve of Fig. 2b and legend for details). The fitted molecular dipole moment is $\mu = 1.025(15) e a_o$, in agreement with the theoretical prediction[16] $\mu = 1.015 e a_o$, where $e$ is the elementary charge, $a_o$ is the Bohr radius, and the number in parentheses indicates the standard uncertainty (or standard deviation of the mean) on the last two digits.

The dipole moments of molecular ions are difficult to measure, and only a few have been determined from the rotational Zeeman effect by laser spectroscopy[4–6]. The technique demonstrated here offers an alternative route to important physical chemistry data, as well as being both conceptually simple and providing an accuracy comparable to the best spectroscopic determinations. Also, because only a single ion is necessary, this technique is applicable to highly reactive molecules or those for which large enough quantities cannot be synthesized for laser spectroscopy.

Because of better statistics and discrimination, we can measure the cyclotron frequency ratio $R_{0,0}$ of the ground state with an uncertainty of $7 \times 10^{-12}$, which includes the statistical and systematic errors from ion–ion interaction and trap field imperfections[7]. Unfortunately, the accuracy of the mass ratio we extract, $R = M[CO^+]/M\left[N_2^+\right] = 0.999\ 598\ 887\ 627(15)$, is limited by our knowledge of $\mu$. Still, the fractional uncertainty of $1.5 \times 10^{-11}$ makes this one of the three most precisely known mass ratios. A measurement or calculation of the electric dipole moment with fractional accuracy of 0.5% would be needed to determine the unperturbed mass ratio from the ground-state cyclotron frequency ratio with the same accuracy as $R_{0,0}$ from $R = M[CO^+]/M\left[N_2^+\right] = 0.999\ 598\ 888\ 635\ (7) - (959 \times \mu^2 \times 10^{-12})$ where $\mu$ is expressed in $e a_o$. After correcting for the mass of the missing electrons[17], and ionization and molecular binding energies[18], we obtain a neutral mass difference $2 \times M[^{14}N] - M[^{16}O] - 12\ \mathrm{u} = 0.011\ 233\ 389\ 32(42)\ \mathrm{u}$ in unified atomic mass units. This mass comparison is metrologically important because it determines the neutral atomic masses $M[^{14}N]$ and $M[^{13}C]$ to fractional accuracies of $\sim 2 \times 10^{-11}$ when combined with previously reported mass comparisons[7,8,19].

The above mass ratio differs from our previously measured value, obtained by alternately trapping and measuring the cyclotron frequencies of the two ions[20], by less than the previous uncertainty of $7 \times 10^{-11}$. We believe that our group's previous measurements[3,20] do not significantly suffer from any systematic error from polarization shifts because the rotational state, and hence the systematic error, was randomized each time a new ion was created by electron impact ionization. Moreover, the ions did not have time to relax to the ground rotational state (the only state possessing a large polarizability) during the subsequent ~10 min over which the cyclotron frequency was measured.

The cyclotron frequency shift reported here is a very general phenomenon affecting all cyclotron frequency comparisons involving polarizable particles. For instance, the most precise test of charge-parity-time (CPT) reversal symmetry using baryons[10] was performed by comparing the charge to mass ratios of the proton $p$ and antiproton $\bar{p}$. The measurement was actually performed by comparing the cyclotron frequencies of $H^-$ and $\bar{p}$. Correcting for the polarization force shift of the $H^-$ ion's cyclotron frequency[10,21] using $\alpha[H^-] = 0.34 \times 10^{-38}\,\mathrm{C\,m^2\,V^{-1}}$ and $B = 5.9\,\mathrm{T}$, the reported ratio changes from $(q[\bar{p}]/m[\bar{p}])/(q[p]/m[p]) + 1 = 0.9(9) \times 10^{-10}$ to a corrected value of $1.6(9) \times 10^{-10}$. Further, uncertainties in the size of the polarization shift of the $SiH^+$ and $SH^+$ molecules are expected to limit the accuracy of the mass comparisons for a new direct test of Einstein's mass–energy relationship $E = mc^2$, achieved by comparing the energy of the $\gamma$-rays emitted in a neutron capture process to the measured mass shift between the isotopes (ref. 9, and J.K.T., S.R., E.G. Myers and D.E.P., manuscript in preparation).

The cyclotron frequency shift presented here can be much larger in other systems. For scale, we consider a large linear molecule with $\mu = 5 e a_o$, $M = 280\,\mathrm{u}$, and the same linear mass density as $CO^+$, measured in the currently attainable magnetic field of $B = 20\,\mathrm{T}$. The fractional cyclotron frequency shift of the ground rotational state would be $\Delta\omega_c/\omega_c \approx 10^{-5}$, gigantic by the standards of state-of-the-art cyclotron frequency comparisons, and within reach of the higher-performance ion cyclotron resonance experiments used for physical or biological chemistry[1]. However, for such a hypothetical molecule, the induced dipole approaches the molecular dipole moment at a cyclotron radius of only $\rho_c^{\mathrm{critical}} \approx 10\,\mu\mathrm{m}$. Above this critical value, the cyclotron frequency shift should roughly fall off from its small orbit value as $\rho_c^{\mathrm{critical}}/\rho_c$. Additionally, such a large molecule in thermal equilibrium would occupy much higher rotational states ($N \approx 25$ being the most likely occupied rotational level at 4 K) possessing smaller polarization shifts than that of the ground state. Therefore, this polarization force might manifest itself mostly as a broadening of the cyclotron resonance in such experiments.

This newly discovered cyclotron frequency shift will need to be carefully accounted for in future high-precision cyclotron frequency comparisons. Also, the demonstrated quantum non-demolition measurement of the rotational state of a single polar molecular could prove useful for high-precision single-molecule spectroscopy—a particularly interesting idea for possible electron dipole moment searches using polar molecules[22]. □

Received 4 April; accepted 25 May 2004; doi:10.1038/nature02682.

1. Marshall, A. G., Hendrickson, C. L. & Shi, S. D. Scaling MS plateaus with FTICR MS. *Anal. Chem.* **74,** 252A–259A (2002).
2. Heninger, M. *et al.* Successive reactions of iron carbonyl cations with methanol. *Int. J. Mass Spectrom. Ion Process.* **199,** 267–285 (2000).
3. Bradley, M. P., Porto, J. V., Rainville, S., Thompson, J. K. & Pritchard, D. E. Penning trap measurements of the masses of $^{133}$Cs, $^{87}$Rb, $^{85}$Rb, and $^{23}$Na with uncertainties ≤ 0.2 ppb. *Phys. Rev. Lett.* **83,** 4510–4513 (1999).
4. Havenith, M., Zwart, E., Meerts, W. L. & ter Meulen, J. J. Determination of the electric dipole moment of $HN_2^+$. *J. Chem. Phys.* **93,** 8446–8451 (1990).
5. Laughlin, K. B., Blake, G. A., Cohen, R. C., Hovde, D. C. & Saykally, R. J. Determination of the dipole moment of $ArH^+$ from the rotational Zeeman effect by tunable far-infrared laser spectroscopy. *Phys. Rev. Lett.* **58,** 996–999 (1987).

6. Linnartz, H., Havenith, M., Zwart, E., Meerts, W. L. & ter Meulen, J. J. Determination of the electric-dipole moment of $KrH^+$. *J. Mol. Spectrosc.* **153,** 710–717 (1992).
7. Rainville, S., Thompson, J. K. & Pritchard, D. E. An ion balance for ultra-high-precision atomic mass measurements. *Science* **303,** 334–338 (2004).
8. VanDyck, R. S., Zafonte, S. L. & Schwinberg, P. B. Ultra-precise mass measurements using the UW-PTMS. *Hyperfine Interact.* **132,** 163–175 (2001).
9. Greene, G. L., Dewey, M. S., Kessler, E. G. & Fischbach, E. Test of special relativity by a determination of the Lorentz limiting velocity — does $E = mc^2$? *Phys. Rev. D* **44,** R2216–R2219 (1991).
10. Gabrielse, G. *et al.* Precision mass spectroscopy of the antiproton and proton using simultaneously trapped particles. *Phys. Rev. Lett.* **82,** 3198–3201 (1999).
11. Wei, H. Q., Han, R. S. & Wei, X. Q. Quantum phase of induced dipoles moving in a magnetic field. *Phys. Rev. Lett.* **75,** 2071–2073 (1995).
12. Bergstrom, I. *et al.* SMILETRAP — A Penning trap facility for precision mass measurements using highly charged ions. *Nucl. Instrum. Methods Phys. Res. A* **487,** 618–651 (2002).
13. Jagod, M. F. *et al.* Infrared spectroscopy of carbo-ions. VI. C-H stretching vibration of the acetylene ion $C_2H_2^+$ and isotopic species. *J. Chem. Phys.* **97,** 7111–7123 (1992).
14. Dixon, T. A. & Woods, R. C. Microwave absorption spectrum of the $CO^+$ ion. *Phys. Rev. Lett.* **34,** 61–63 (1975).
15. Townes, C. H. & Schawlow, A. L. *Microwave Spectroscopy* (Dover Pub. Inc., New York, 1975).
16. Martin, P. A. & Feher, M. CASSCF calculations of the multipole moments and dipole polarizability functions of the $X^2\Sigma^+$ and $A^2\Pi$ states of $CO^+$. *Chem. Phys. Lett.* **232,** 491–496 (1995).
17. Beier, T. *et al.* New determination of the electron's mass. *Phys. Rev. Lett.* **88,** 011603 (2002).
18. Huber, K.P. & Herzberg G. (data prepared by Gallager, J.W. & Johnson, R. D.) *"Constants of Diatomic Molecules", NIST Chemistry WebBook, NIST Standard Reference Database Number 69* (eds Lindstrom, P.J. & Mallard, W. G.) (National Institute of Standards and Technology, Gaithersburg, MD, 2003); ⟨http://webbook.nist.gov⟩ (2003).
19. Audi, G., Wapstra, A. H. & Thibault, C. The AME2003 atomic mass evaluation (II). Tables, graphs and references. *Nucl. Phys. A* **729,** 337–676 (2003).
20. DiFilippo, F., Natarajan, V., Boyce, K. R. & Pritchard, D. E. Accurate atomic masses for fundamental metrology. *Phys. Rev. Lett.* **73,** 1481–1484 (1994).
21. Bhatia, A. K. & Drachman, R. J. Polarizability of helium and the negative hydrogen ion. *J. Phys. B* **27,** 1299–1305 (1994).
22. Kozlov, M. G. & DeMille, D. Enhancement of the electric dipole moment of the electron in PbO. *Phys. Rev. Lett.* **89,** 133001 (2002).


**Acknowledgements** We thank E.G. Myers, G.J. Sussman, J. Wisdom and W. Ketterle for useful discussions. This work was supported by the National Science Foundation and a National Institutes of Standards and Technology Precision Measurement Grant. S.R. acknowledges support from the Fonds pour la Formation de Chercheurs et l'Aide à la Recherche.

**Competing interests statement** The authors declare that they have no competing financial interests.

**Correspondence** and requests for materials should be addressed to J.K.T. (jkthomps@alum.mit.edu).

# Single-crystal metallic nanowires and metal/semiconductor nanowire heterostructures

**Yue Wu[1]*, Jie Xiang[1]*, Chen Yang[1], Wei Lu[1] & Charles M. Lieber[1,2]**

[1]*Department of Chemistry and Chemical Biology; and*
[2]*Division of Engineering and Applied Sciences, Harvard University, Cambridge, Massachusetts 02138, USA*

* These authors contributed equally to this work

**Substantial effort has been placed on developing semiconducting carbon nanotubes[1–3] and nanowires[4] as building blocks for electronic devices—such as field-effect transistors—that could replace conventional silicon transistors in hybrid electronics or lead to stand-alone nanosystems[4,5]. Attaching electric contacts to individual devices is a first step towards integration, and this step has been addressed using lithographically defined metal electrodes[1–4,6–8]. Yet, these metal contacts define a size scale that is much larger than the nanometre-scale building blocks, thus limiting many potential advantages. Here we report an integrated contact and interconnection solution that overcomes this size constraint through selective transformation of silicon nanowires into metallic nickel silicide (NiSi) nanowires. Electrical measurements show that the single crystal nickel silicide nanowires have ideal resistivities of about 10 μΩ cm and remarkably high failure-current densities, $>10^8$ A cm$^{-2}$. In addition, we demonstrate the fabrication of nickel silicide/silicon (NiSi/Si) nanowire heterostructures with atomically sharp metal–semiconductor interfaces. We produce field-effect transistors based on those heterostructures in which the source–drain contacts are defined by the metallic NiSi nanowire regions. Our approach is fully compatible with conventional planar silicon electronics and extendable to the 10-nm scale using a crossed-nanowire architecture.**

Our focus on NiSi nanowires is motivated by previous investigations of metal silicides, which can exhibit low resistivity, compatibility with conventional silicon manufacturing, and the ability to form ohmic contacts to both p- and n-type silicon[9]. We prepared NiSi nanowires using an approach (Fig. 1a) involving deposition of nickel metal onto single-crystal Si nanowires[10,11], solid-state reaction at 550 °C to form NiSi, followed by removal of remaining metal by wet etching (see Methods). Low-resolution transmission electron microscopy (TEM) studies (Fig. 1b) of materials prepared in this

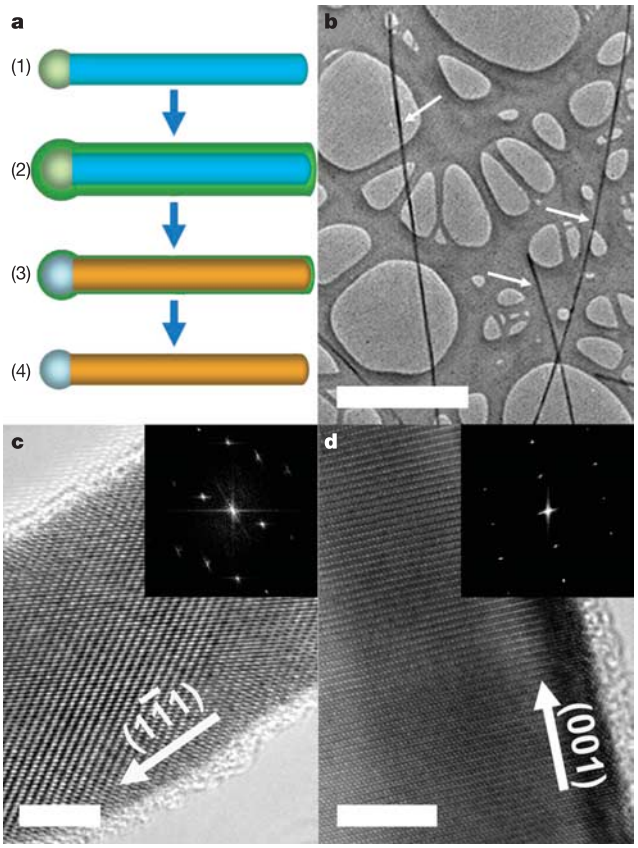


**Figure 1** Preparation and structural characterization of single-crystal NiSi nanowires. **a**, Preparation of single-crystal NiSi nanowires. (1) Si nanowires (blue) of uniform diameter are (2) coated with Ni metal (green) to a total thickness comparable to the Si nanowire diameter, (3) reacted at 550 °C to form NiSi nanowires (brown), and then (4) etched to remove any excess Ni metal. **b**, TEM image of three NiSi nanowires prepared using Si nanowires with an average diameter of about 20 nm. The NiSi nanowires are highlighted by white arrows; scale bar is 1 μm. **c** and **d**, High-resolution TEM images of single-crystal NiSi nanowires. **c**, TEM image of a 20-nm NiSi nanowire prepared using Si nanowires of average diameter 20 nm. The white arrow indicates the growth front of the nanowire. Inset, two-dimensional Fourier transform of the image showing the $[10\bar{1}]$ zone axis of NiSi. **d**, Image of a 32-nm NiSi nanowire prepared using Si nanowires of average diameter 30 nm. The white arrow indicates the growth front of the nanowire. Inset, two-dimensional Fourier transform of the image depicting the $[2\bar{1}0]$ zone axis of NiSi. The scale bars in **c** and **d** are 5 nm.